HHS Public Access

Author manuscript

Comput Biol Med. Author manuscript; available in PMC 2017 March 01.

Published in final edited form as:

Comput Biol Med. 2016 March 1; 70: 210–219. doi:10.1016/j.compbiomed.2016.01.019.

Morphometric analysis of calcification and fibrous layer thickness in carotid endarterectomy tissues

Richard I. Han, PhD[1,4], **Thomas M. Wheeler, MD**[3], **Alan B. Lumsden, MD**[2], **Michael J. Reardon, MD**[2], **Gerald M. Lawrie, MD**[2], **Jane K. Grande-Allen, PhD**[4], **Joel D. Morrisett, PhD**[1], and **Gerd Brunner, PhD**[1,2]

[1]Division of Atherosclerosis and Vascular Medicine, Department of Medicine, Baylor College of Medicine, Houston, Texas

[2]Methodist DeBakey Heart and Vascular Center, Houston Methodist Hospital, Houston, Texas

[3]Department of Pathology & Immunology, Baylor College of Medicine, Houston, Texas

[4]Department of Bioengineering, Rice University, Houston, Texas

Abstract

Background—Advanced atherosclerotic lesions are commonly characterized by the presence of calcification. Several studies indicate that extensive calcification is associated with plaque stability, yet recent studies suggest that calcification morphology and location may adversely affect the mechanical stability of atherosclerotic plaques. The underlying cause of atherosclerotic calcification and the importance of intra-plaque calcium distribution remains poorly understood.

Method—The goal of this study was the characterization of calcification morphology based on histological features in 20 human carotid endarterectomy (CEA) specimens. Representative frozen sections (10μm thick) were cut from the common, bulb, internal and external segments of CEA tissues and stained with von Kossa's reagent for calcium phosphate. The morphology of calcification (calcified patches) and fibrous layer thickness were quantified in 135 histological sections.

Results—Intra-plaque calcification was distributed heterogeneously (calcification %-area: bulb segment: 14.2±2.1%; internal segment: 12.9±2.8%; common segment: 4.6±1.1%; p=0.001). Calcified patch sizes ranged from <0.1mm^2 to >1.0mm^2, and were found in 20 CEAs. Calcified patches were most abundant in the bulb and least in the common segment (bulb n=7.30±1.08; internal n=4.81±1.17; common n=2.56±0.56; p=0.0007). Calcified patch circularity decreased with increasing size (<0.1mm^2=0.77±0.01, 0.1–1mm^2=0.62±0.01, >1.0mm^2=0.51±0.02; p=0.0001). A reduced fibrous layer thickness was associated with increased calcium patch size (p<0.0001).

Address for Correspondence: Gerd Brunner, PhD, 6565 Fannin St., Fondren-Brown-Alkek Tower, Suite A679, MS A-601, Houston, Texas, Tel: (713) 798-3438, Fax: (713) 798-8039, gbrunner@bcm.edu.

Conflicts of interest: None Declared.

Conclusions—In advanced carotid atherosclerosis, calcification appears to be a heterogeneous and dynamic atherosclerotic plaque component, as indicated by the simultaneous presence of few large stabilizing calcified patches and numerous small calcific patches. Future studies are needed to elucidate the associations of intra-plaque calcification size and distribution with atherothrombotic events.

Keywords

carotid endarterectomy; calcification; image analysis; carotid bifurcation; fibrous layer

1. Introduction

The presence of arterial calcification is a prominent feature in advanced atherosclerotic lesions. Calcified plaques have been located in multiple arterial beds and the strength of the association with mortality depends on the vascular bed (1). In particular, coronary calcifications have been identified as an independent and additive predictor of incident nonfatal and fatal cardiovascular events and stroke (2–4). However, fewer studies have assessed calcified plaques in the carotids, including the Diabetes Heart Study that identified carotid artery calcification as a significant predictor of cardiovascular events (5). Although patients with arterial calcifications have an increased risk of cardiovascular events, the exact role that calcification plays in atherosclerosis remains incompletely characterized and controversial with respect to plaque stability. It is believed that atherogenic growth factors and cytokines induce among other changes, vascular smooth muscle cell (VSMC) migration and proliferation. Over time a subset of VSMCs may transdifferentiate into calcified vascular cells (CVCs), an osteogenic phenotype that contributes to plaque calcification (6–8). In our previous studies, lysophosphatidylcholine, a product of oxidized phosphatidylcholine hydrolysis has been found in carotid endarterectomy (CEA) atheroma and was identified as a candidate for stimulating VSMCs to transdifferentiate into CVCs (9, 10). However, the current understanding of the atherosclerotic calcification process does not account for the observed heterogeneous distribution of intra-plaque calcification (11). Moreover, sites of calcification have been implicated in biomechanical changes of the arterial wall. Although previous analyses have associated calcified atherosclerotic lesions with plaque stability (12, 13), recent studies indicate that calcification size and location are important determinants of plaque rupture risk (14, 15). However, the exact mechanism of atherosclerotic calcification including the spatial distribution and size of calcific regions within atherosclerotic lesions remains incompletely understood (16).

The underlying hypothesis of this study was that the characterization of calcification morphology will lead to a clearer understanding of the mechanism of plaque formation and stability. The aim of this study was to provide a detailed characterization of calcification morphology based on histological features in human CEA specimens. Emphasis has been focused on calcified patch size and shape, particularly their relation to tissue anatomical locations, lumen morphologies and fibrous layer thickness.

2. Materials and Methods

2.1 Tissue collection

CEA tissues were collected from patients undergoing surgery at the Houston Methodist Hospital. The tissues were obtained 3 to 6 hours after resection and immediately immersed in PBS/glycerol (50:50) and stored at −20°C until use. This study complied with local institutional human research review board and established ethical guidelines.

2.2 Histochemistry

Twenty CEA tissues, 13 right (Rt) and 7 left (Lt) were scanned with a high-resolution micro-computed tomography (CT) (Inveon PET/Spect/CT, Siemens, PA, USA) using Inveon Research Workplace software (Siemens, Malvern, PA; additional details can be found elsewhere (11)). The tissues were frozen in OCT compound (Sakura Finetek, Torrance, CA). The micro-CT images were used to guide the selection of frozen sections (10μm thick). Representative locations (internal/external, bulb and common segments) of the CEA tissues were collected. Depending on the size and extent of calcification, 5 to 10 different representative locations were selected along each tissue. Serial cross sections in that particular location were cut and stained with von Kossa's reagent for calcium phosphate, Masson's Trichrome reagent to distinguish collagen from fibrin, and Oil Red O reagent for lipids (Figure 1).

2.3 Image acquisition

Microphotographs of whole slide tissue images were acquired using a Pathscan Enabler IV microscope slide scanner (Meyer Instruments, Houston, TX) at 7,200 dpi. The digitized images of sections were warped when necessary to achieve closure of the surgical slit on the vessel wall (MorphAge, Creaceed Inc., Mons, Belgium). The histological images were arranged in a panel in the order of their relative positions along the tissue (Figure 1). For high magnification studies, the histological slides were examined under a bright field microscope (Leica, Buffalo Grove, IL). In one CEA tissue, the slides were scanned with a high-end whole slide scanner (Panoramic 250, PerkinElmer, Waltham, MA) in order to document very small calcium particles on the micro scale.

2.4 Image analysis

The morphological analysis was performed on a Macintosh MacBook Air (Apple Computer, Cupertino, CA) using the public domain ImageJ software (National Institutes of Health, Bethesda, MD). von Kossa stained sections representing the transverse area of the tissues were subjected to image analysis. The captured image was calibrated with a 2 mm stage micrometer. The outline of the entire tissue, the lumen, and visualized calcium patches were traced carefully (Figure 2). Calcified patches were identified as the area of calcification. Cross-sectional tissue and lumen area, perimeter of lumen and area of calcium deposit were determined. In addition, shape descriptors including [circularity = $4\pi(\text{area}/\text{perimeter}^2)$], [aspect ratio = major axis/minor axis], and [roundness = $4\times\text{area}/\pi\times(\text{major axis}^2)$] were obtained for each calcified patch (Supplemental Table 1). From the measured lumen perimeter, the radius was calculated from the equation [perimeter = 2π r]. Hypothetical

lumen, representing a patent circular lumen was constructed using the radius value from the equation [area = πr^2]. The true lumen area was compared to the hypothetical circular lumen and expressed as a percentage ratio to describe shape deviation. The total calcium phosphate burden per tissue section was reported as a percentage of calcification area per tissue area. Using the lumen center of mass as a reference point, a line was drawn through the mid-point of each calcium patch to the outer surface of the CEA tissue. The thickness of the fibrous layer was measured along a line from the lumen surface to the edge of the calcium boundary.

To study the very small calcified particles, the scanned image data set was viewed in Panoramic Viewer software (3DHistech, Budapest, Hungary). The area of interest was converted to TIFF format. The image was then imported into ImageJ and the region of interest was delineated. The very small calcified particles were selected by applying a color density threshold then their circularity values were determined.

2.5 Radial distribution of calcified patches

For the 9 CEA tissues containing both internal and external branches that display visible histology, the calcified patch angle occupations were morphed into a 360° clock. The centroids, defined as the center points of the internal and external lumens, were determined in their x and y coordinates. A line connecting the centroids of the two lumens was used as a reference line to measure locations of calcifications in degrees. Angular occupation by the calcified patches was measured from lumen centroid using the reference line as 0°. This was represented by an arc around the concentric circle (Omni Graffle Pro, Seattle, WA). The arcs in the same concentric circle represented the calcified patches located on the same tissue section. The outer rim represents the proximal side, and the inner rim the distal side. A perpendicular line intersects the reference line at the internal lumen centroid that divides the tissue into two halves, an inner half facing the external segment and an outer half facing away from the external segment. Calcification in each half was expressed as a percentage of total calcification area.

2.6 Immunohistochemistry

Three out of 20 frozen CEA tissues and 1 additional paraffin-embedded CEA tissue were selected for study. Tissue sections first underwent an antigen retrieval process. Sections were heated to 95°C in citric acid (0.01M, pH 6.0) prior to antibody detection. A standard two level antibody labeling system plus diaminobenzidine as the chromagen was used. Sections were pretreated with 1% hydrogen peroxide in PBS solution to inhibit endogenous peroxidase activities. Mouse anti-human monoclonal antibodies against α-smooth muscle actin (DAKO N-1584, Carpinteria, CA), CD 68 (DAKO N1577, Carpinteria, CA), osteopontin (R&D MAB-1433, Minneapolis, MN), osteocalcin (R&D MAB-1419, Minneapolis, MN) and osteonectin/SPARC (R&D MAB-941, Minneapolis, MN) were applied to the tissue sections at concentrations recommended by the suppliers for immunohistochemistry identification (Supplemental Figure 1). Biotinylated antibodies (Vector Laboratories, Burlingame, CA) against mouse IgG were applied as secondary antibodies. An avidin-biotin peroxidase system was used according to supplier's

recommendation (ABC kit, Vector Laboratories, Burlingame, CA). Sections were counterstained with Mayer's hematoxylin.

2.7 Semi-quantitative analysis of collagen and non-collagen proteins

Three CEA samples were used: one frozen and two paraffin-embedded. The technique utilized the collagen-specific Sirius Red stain and non-collagen protein Fast Green stains. The procedure was performed in accord with the supplier's recommendation (Chondrex Inc., Redmond, WA, USA). Essentially, the dye solution was applied to the tissue sections and the excess dye was rinsed off with water. The bound dye was then extracted and its OD reading was taken at 540 nm and 605 nm by spectrophotometry (NanoDrop 100, Thermo Scientific, Waltham, MA). The amount of collagen and non-collagen protein were calculated from the formulae provided by the supplier.

2.8 Statistical analysis

The calcified patch number and calcification area were normalized to section numbers for each segment. In calcified particle shape analysis, the calcified patches were grouped according to their sizes: small ($<0.1mm^2$), medium ($0.1–1mm^2$) and large ($>1.0mm^2$). The fibrous layer thickness was expressed as a fraction of the vessel wall thickness, in order to normalize for inter-sample comparisons. Correlation was determined from a bivariate plot with the best line fit option using Prism statistical software (GraphPad Prism V.5, La Jolla, CA). Fisher's exact test was used to analyze categorical data. The inferential statistical analysis involved one-way analysis of variance (ANOVA) testing. The results were presented as mean ± standard error (SE). The significance of any difference was then checked with the non-parametric Wilcoxon/Kruskal-Willis ranked sum test, with a p-value <0.05 considered statistically significant. Where ANOVA detected significant difference, inter-group differences were compared using the post-hoc Tukey-Kramer pairwise analysis (JMP version 8.0.2, SAS, Cary, NC). In a section with three visible calcium patches, all measurements were performed in triplicate to assess reproducibility. Intraclass correlation coefficient (ICC) analysis was used to assess reproducibility of calcified patch measurements (SPSS, IBM, Armonk, NY).

3. Results

A total of 631 calcified patches were analyzed in 135 histological sections obtained from 20 CEA tissues (Figure 1). Calcified patch sizes ranged from smaller than 0.1 mm^2 to larger than 1 mm^2 which were present in all 20 CEA tissues, and covered a total area of up to 56.9% of the tissues' cross-sectional area (calcified patch size range: 0.0013–10.97 mm^2). Nine CEA tissues out of 20 featured both internal and external branches. Calcification was found in all internal branches, but in only 3 of the external branches ($p<0.001$).

3.1 Fibrous layer

The mean fibrous layer was found to be significantly thicker in the bulb segment in comparison to the internal and common segments ($p=0.01$, Figure 3). The fibrous layer thickness was inversely related to the calcium patch size (linear fit, $p<0.0001$, Figure 3B), and this inverse relationship was sustained in all three segments (internal, $p<0.0001$; bulb,

p<0.0001; and common, p=0.0025). The mean fibrous layer thickness in the >1.0mm^2 sized calcium group was 1.048mm, thinner and significantly different from <0.1mm^2 (1.387mm) and 0.1–1.0mm^2 (1.418mm), (p=0.0189). The fibrous layer ratio in the >1.0mm^2 size group was lower and significantly different from the two smaller sized groups (Figure 3C).

3.2 Calcified patch number

When the Lt and Rt CEAs were combined, the mean number of calcified patches was highest in the bulb segment (7.30±1.08), followed by the internal segment (4.81±1.17) and the common segment (2.56±0.56) (p=0.0007; Figure 4, and Supplemental Figure 2). The calcified patch number in the bulb segment was significantly different from calcified patch numbers in both internal and common segments (p=0.0039). There was no difference in total calcified patch numbers between Lt CEAs (mean=5.19±1.02) and Rt CEAs (mean=4.73±0.75; p=0.36). When comparing the calcified patch numbers in each of the three segments, no significant differences were found between Lt CEAs and Rt CEAs. In the section with three calcium patches, the measurements were all below a 5% margin of error from each other and from their mean, and reproducibility was excellent (ICC=0.99, and 0.99, respectively). Supplemental Table 2 provides complete information regarding the morphological measurements of all calcified patches.

3.3 Calcification area

In a pooled analysis of Lt and Rt CEAs, the bulb segment contained the highest calcification % area (14.2±2.1%). This was followed by the internal segment (12.9±2.8%); and the common segment had the lowest amount of calcification (4.6±1.1%, p=0.001; Figure 4B). The calcification % area in the bulb segment was three-fold higher than in the common. The total calcification area tended to be higher in Lt CEAs (mean=14.0±2.2%) compared to Rt CEAs (mean=8.8±1.6%, p=0.067).

3.4 Ratio: measured lumen area to hypothetical lumen area

The luminal area ratio in the bulb segment was significantly lower in the bulb segment (64.1±2.5%) compared to the internal (72.7±2.4%), and the common (73.1±3.1%, p=0.018; Figure 4C). Overall, there was no difference in the ratio between Lt CEAs (68.4±2.8%) and Rt CEAs (70.8±2.0%, p=0.47).

3.5 Geometric characteristics of calcified patches

The mean circularity value decreased significantly with increasing size of the calcified patches (<0.1mm^2=0.77±0.01, 0.1–1mm^2=0.62±0.01, and >1.0mm^2=0.51±0.02; p=0.0001; Figure 5). The circularity value for each calcified patch size group was significantly different from the other two groups.

The mean aspect ratio in the small patch size group (<0.1mm^2=1.78±0.08) was significantly lower than the medium patch size group (0.1–1mm^2=2.44±0.11), and the large patch size group (>1.0 mm^2=2.41±0.14, p=0.0001; Figure 5B).

The mean roundness (a measure of eccentricity) in the small patch size group (<0.1mm^2=0.62±0.02) was significantly higher than in the medium patch size group (0.1–1mm^2=0.49±0.03) and large patch group (>1.0 mm^2=0.48±0.02, p=0.0001; Figure 5C).

3.6 Correlations: calcification area vs. tissue area; calcification area vs. lumen area & tissue area vs. lumen area

In 7 of the 20 CEA tissues, there was a significant correlation between calcified area and total tissue area. However, when the calcified area was plotted against the lumen area, only one of the 20 CEA tissues indicated a significant correlation using the best line fit function. Bivariate plots between tissue area and lumen area showed a significant correlation in three CEA tissues.

3.7 Correlation: calcified patch area vs. calcified patch perimeter

The correlations of calcified patch area vs. calcified patch perimeter were high in all three sized patch groups (<0.1mm^2, r=0.97; 0.1mm^2–1.0mm^2, r=0.88; and >1.0mm^2, r=0.93; Supplemental Figure 3).

3.8 Very small calcified particles

Under a bright field microscope, calcified particles appeared as very small punctuate dots (Figure 6). At high magnification (20X lens setting), these calcified particles were round. A high-end slide scanner [3DHistech Pannoramic Scanner, Perkin Elmer] with z-depth focusing revealed the locations of these very small calcified particles which tended to group in diffuse clusters. We did not observe any preferential location distribution with respect to nearby larger calcified patches, as illustrated in Figure 6.

In a simulation experiment, 203 (88%) of 230 calcified particles were detected and a circularity score of 1 (perfect circle) was observed. The mean circularity value for the 230 very small-calcified particles was 0.97.

3.9 Radial distribution of calcified patches

The radial distribution of calcified patches is presented in Figure 7. In the external branch, the half facing the internal branch was the preferential site for calcification. In the internal branch, the half of the vessel wall facing the external branch was the preferred site for calcification, since the majority of calcified patches were located in that space. In Lt CEA, inner calcification area=68% vs. outer calcification area=32%, p=0.015. In Rt CEA, inner calcification area=80% vs. outer calcification area=20%, p=0.0003.

3.10 Immunohistochemistry

Osteopontin positive staining was observed in the regions immediately adjacent to calcified patches. Osteonectin staining was more diffuse and loosely scattered in the tissue. Osteocalcin was closely associated with calcified patches; the staining appeared more diffuse and could be observed within the calcified area (Supplemental Figure 1). The α-SMA staining of the sections was heterogeneous. Positive staining in the sub-endothelial space of a thickened fibrous layer was readily apparent. α-SMA positive staining near the intimal-medial boundary had a more diffuse appearance. Occasionally, the α-SMA stain was

found adjacent to calcified patches. The presence of macrophages was indicated by sparsely but focal CD68 staining; positive staining extended deep into the tissue and localized toward the medial layer borderline. CD68 staining could also be detected in the region flanking the lipid core (data not shown).

3.11 Semi-quantitative collagen and non-collagen protein

Collagen was examined in a selection of nine sections from three CEA tissues representing the internal, bulb, and common segments. The collagen in frozen tissue sections was low and their collagen/non-collagen protein ratios were between 1.9% and 4.0%. In contrast, the collagen, non-collagen protein ratios in paraffin-embedded CEAs were between 11.5% and 14.8%.

4. Discussion

In this study, we have found that calcified patches of various sizes are present in 20 CEA tissues. The internal segments were more prone to calcification than external segments. Calcified patch size ranged from smaller than 0.1 mm^2 to larger than 1 mm^2. These patches could be found in each of the 20 CEA tissues. Our analysis shows that calcified patch number, calcification area, and lumen area were highest in the bulb segment, followed by the internal segment, and lowest in the common segment of CEA tissues. An increase in calcified patch size was associated with a more irregular shape and larger eccentricity. Larger calcified patches were inversely proportional to fibrous layer thickness.

4.1 Histological morphology

Atherosclerotic plaque is a heterogeneous structure resulting from complex cellular interactions in the intimal wall. The accumulation of cholesteryl ester in low-density lipoprotein (LDL) particles is a hallmark of atherosclerosis. Over time oxidized-LDL (oxLDL) and lysophosphatidylcholine can promote calcification in vascular interstitial cells (9, 17). Advanced atherosclerotic plaques are characterized by the formation of a fibrous cap which encages the lipid core atheroma and the presence of calcification which results from the deposition of calcium phosphate crystals (typically as hydroxyapatite) in the vessel wall. Atherogenic growth factors and proinflammatory cytokines are believed to initiate vascular smooth muscle cell migration and proliferation which can transdifferentiate into calcified vascular cells, a known osteogenic phenotype that is implicated in plaque calcification (18, 19). In this study, calcified patches of various sizes were found in each of the CEA tissues. The different stages of calcification have been described as dispersed ‘stippling’, ‘morula’, and ‘solid’ deposits, representing a progressive increase in patch size that is consistent with our results (20). It was found that the early stippling was in the area peripheral to small pools of extracellular lipids, fibrous caps, and shoulder regions of atherosclerotic lesions. We found similar distributions but also identified the bifurcation segment as the predominant location of calcifications. The early stage of calcification was closely associated with mast cells and macrophages (20). Previously, von Kossa’s stain has been used to study CEA tissues for the identification of calcified patches (20, 21). von Kossa’s reagent is a conventional histochemical stain used to quantify mineralization in tissues (22). This reagent was the stain of choice because of its high contrast in the downstream image

analysis process instead of calcium specific Alizarin Red S stain. Recent studies on calcific lesions in aortae and mitral valves using electron microscopy have identified crystalline hydroxyapatite among micro-spherical particles in tissues, suggesting that calcium and phosphate rich spherical particles are the first mineralized structures to appear in ectopic tissues (23, 24). Previous descriptions of the smallest calcified structures, also referred to as microcalcifications (20) (23) are consistent with the morphology of the "very small calcified particles" described in this study (Figure 6C). We have found that the very small calcified particles are almost exclusively round in 2D histology sections (Figure 6C). Earlier studies have suggested that the action of Lipoprotein-associated phospholipase A2 (Lp-PLA2) on oxLDL produce lyso-phosphatidylcholine, an atherogenic agent which can, in turn, induce VSMCs to differentiate into calcifying vascular cells in vitro (9, 10). Our group has shown previously that levels of oxLDL and Lp-PLA2 activities were high in the bifurcation segment of CEA tissues (25), which may give rise to the very small calcified particles observed in this study. The smallest quantified calcified patches in this study are larger than the microcalcifications of coronary lesions reported in the study by Kelly-Arnold et al (14). However, the very small calcified particles shown in Figure 6C are of comparable size to the microcalcifications reported by Kelly-Arnold et al (14), suggesting similar underlying calcification processes in the carotid and coronary arteries. Although, we have quantified these very small calcified particles only at one sample location, their distribution density seems to be in agreement with similar observations (14). Our limited analysis of these microcalcifications indicates a round appearance and no co-localization with larger calcified patches. A systematic quantification of microcalcifications in atherosclerotic plaques is required to confirm this observation.

4.2 Calcification morphology

The calcified patch shape descriptors reported in this study, indicate that nascent very-small calcified particles are round in shape (circularity=1). Larger calcified particles featured a distinct shape as indicated by an increased aspect ratio, and a more irregular outline. Conceivably, the osteogenic proteins, together with calcium-preferred binding templates including collagen and elastin, could influence the direction and kinetics of the calcified particle growth. Interestingly, the aspect ratio is larger and roundness is decreased for larger versus smaller particles, indicating distinct changes in the morphology of calcifications (Supplemental Table 1). The largest difference was found between the $<0.1mm^2$ size group and $0.1–1.0mm^2$ size group, indicating a distinct shape change in eccentricity. It has been hypothesized that the small rounded particles fuse with close neighbors to form larger particles (26), which could explain our observations (Figure 5C and Supplement Figure 3).

4.3 Distribution of calcified patches

In our study, calcified patch numbers and calcified area both were found to be highest in the bulb segment, followed by the internal segment and the common segment. These results are consistent with previous reports (27). In the internal branch, the distribution pattern was not immediately apparent due to the complexity and extent of calcification in some CEA tissues. However, calcified patches appear to be localized within the half of the internal branch facing the external branch, as illustrated in Figure 7. The tendency for plaques to form at the carotid artery bifurcation has been attributed to disturbed flow and low wall shear stress (27)

(28). The distribution of calcification sites may be linked to carotid plaque stability (29). To our knowledge, this study is the first to investigate the radial distribution of calcified patches within the vessel wall at the carotid bifurcation. Whether this observation is due to hemodynamic effects or part of the atherosclerosis progression, will require further study.

Previous studies have focused on the modeling of atherosclerotic plaque in the vessel wall and its effect on hemodynamics (30). Vessel wall remodeling in atherosclerosis may involve both positive (enlargement) remodeling and negative (shrinkage) remodeling (31). In this study, the lumen was found to deviate from the circular patent hypothetical lumen which was highest in the bulb segment. The calcified patch size and abundance were also highest in the bulb area, yet a correlation between lumen area and calcified patches was not established. Moreover there was no correlation between total tissue area and lumen area. It is not clear whether a change in lumen area and lumen shape has a direct relation to calcification (32). The lack of a correlation could also be due to the ex vivo nature of this study resulting in significant deformation of the luminal area due to resection of the CEA tissues and the histological analysis. Our findings on the distribution of carotid calcification will need to be confirmed in vivo with non-invasive imaging modalities such as CT or MRI, both of which have shown good agreement with histology for the quantification of arterial calcification (33).

Human medial calcification, also known as Mönckeberg's sclerosis is a common disease seen in diabetic individuals (34). The condition leading to calcification in the elastin rich medial layer of lower limbs has been associated with an increased risk of cardiovascular events. Unlike carotid intimal vascular calcification, as shown in this study, medial calcification is likely not associated with lipids and macrophages and considered independent of atherosclerosis. However, during the calcification process, both types of calcification share a similar cellular transformation, involving smooth muscle actin-positive osteoblast-like cell activities and up-regulation of a class of osteogenic proteins resembling ossification (35), and resulting in calcium hydroxyapatite formation (36).

4.4 Connective tissues

Collagen is highly abundant in the CEA tissue of this study, as visualized with Masson's trichrome. However, Sirius red and Fast Green staining showed in our results that collagen accounted for less than 20% of all non-collagen proteins. Collagen is present in the matrices of all three major skeletal tissue calcification structures: bone, cartilage and dentin (37). It has been shown that the 640Å banded collagen can nucleate apatite from a metastable solution of calcium and phosphate. In other studies, elastin has been observed as a predominant site of calcification in aortic wall tissue (38). The strong association of atherosclerotic plaque with collagen content and fragmented elastin has recently been reported in a mouse model (39). Significantly, it appears that lipid accumulation in human CEA is located near the elastin-rich medial layer, an area coinciding with some early small calcification region. It is unknown whether the hydrophobic nature of elastin imparts higher affinity for hydrophobic lipids. Fibrosis and calcification are part of the extracellular matrix remodeling process counteracting the degradation of extracellular matrix by matrix metalloproteinases (40). However, based on our results which indicate a correlation between

calcification area and total tissue area, it is conceivable that calcification and fibro-elastin proliferation are two independent processes; that can occur concurrently or independently in a diseased state.

4.5 Fibrous layer

We have observed an inverse relationship between fibrous layer thickness and calcified area. The exact role that calcification plays in the formation of atherosclerotic plaque remains controversial. It has been shown that calcification does not contribute to fibrous cap rupture (12), whereas other studies have reported potentially destabilizing effects of fibrous cap microcalcifications (15). Although these findings suggest that both the size and location of calcification is of importance for plaque stability, additional studies are needed to assess the interrelationship between intra-plaque calcification and fibrous layer stability. Fibrous cap thickness (FCT) has been identified as an important determinant of plaque rupture risk. Fibrous caps get thinner due to continued influx and activation of macrophages and the release of metalloproteinases (MMP) and other proteolytic enzymes and plaques become vulnerable when the FCT<65 microns (41). Asabella et al. have studied inflamed vulnerable carotid plaques using 18F-fluorodeoxyglucose positron emission tomography/computer tomography (18F-FDG PET/CT) (42). Their results indicate that the target background ratio is a reliable measure of plaque inflammation when compare with optical microscopy and immunohistochemistry of CEA tissues. In our study, CD68-stained areas (marker of macrophages and inflammation) were flanking lipid-rich regions. We also found that positive α-SMA staining was located in the sub-endothelial space of thickened fibrous layers and occasionally adjacent to calcified patches.

4.6 Limitations

CEA tissues were collected anonymously and therefore it was not possible to compare tissue calcification with patient demographics or clinical information. However, since the CEA anatomy (i.e. common, internal, external, and bulb segments) of carotid endarterectomy tissue was well defined, it was possible to compare calcification distribution and abundance among these tissue segments. Patients undergoing carotid endarterectomy represent a select at risk group of individuals with high grade carotid artery stenosis. Therefore, the degree of calcification reported in this study may not be reflective of the general population with carotid artery disease. A technical limitation of the study was the loss of calcification from some of the frozen sections. In many cases this could be overcome by tracing the perimeter of the calcified cavity. Finally, there was some distortion of the morphology of frozen sections. This was largely overcome by warping the tissue images so as to bring the edges of the surgical slits into proper juxtaposition.

5. Conclusion

Calcification is abundant in carotid endarterectomy tissues and is located predominantly in the bulb. The internal CEA segment is more prone to calcification than the external. The morphology of calcified patches changes significantly with patch size and thinner fibrous layers are associated with larger calcified patches.

Supplementary Material

Refer to Web version on PubMed Central for supplementary material.

Acknowledgments

The authors thank Ms. Iou Chen, MS, for her dedicated technical support, and Perkin Elmer 3D-Histotech Division for sharing the imaging equipment. This work was supported in part by National Institutes of Health (NIH) grants T32HL07812, and R21 HL104377. GB was supported in part by an American Heart Association (AHA) award (13BGIA16720014) and an NIH K25 award (K25HL121149). JDM was supported in part by NIH grant (HL63090).

References

1. Allison MA, Hsi S, Wassel CL, Morgan C, Ix JH, Wright CM, et al. Calcified atherosclerosis in different vascular beds and the risk of mortality. Arteriosclerosis, thrombosis, and vascular biology. 2012; 32(1):140–6.
2. Shaw LJ, Raggi P, Schisterman E, Berman DS, Callister TQ. Prognostic value of cardiac risk factors and coronary artery calcium screening for all-cause mortality. Radiology. 2003; 228(3):826–33. [PubMed: 12869688]
3. Vliegenthart R, Hollander M, Breteler MM, van der Kuip DA, Hofman A, Oudkerk M, et al. Stroke is associated with coronary calcification as detected by electron-beam CT: the Rotterdam Coronary Calcification Study. Stroke; a journal of cerebral circulation. 2002; 33(2):462–5.
4. Budoff MJ, Nasir K, McClelland RL, Detrano R, Wong N, Blumenthal RS, et al. Coronary calcium predicts events better with absolute calcium scores than age-sex-race/ethnicity percentiles: MESA (Multi-Ethnic Study of Atherosclerosis). Journal of the American College of Cardiology. 2009; 53(4):345–52. [PubMed: 19161884]
5. Cox AJ, Hsu FC, Agarwal S, Freedman BI, Herrington DM, Carr JJ, et al. Prediction of mortality using a multi-bed vascular calcification score in the Diabetes Heart Study. Cardiovascular diabetology. 2014; 13:160. [PubMed: 25496604]
6. Prabhakaran S, Singh R, Zhou X, Ramas R, Sacco RL, Rundek T. Presence of calcified carotid plaque predicts vascular events: the Northern Manhattan Study. Atherosclerosis. 2007; 195(1):e197–201. [PubMed: 17482197]
7. Vattikuti R, Towler DA. Osteogenic regulation of vascular calcification: an early perspective. American journal of physiology Endocrinology and metabolism. 2004; 286(5):E686–96. [PubMed: 15102615]
8. New SE, Aikawa E. Cardiovascular calcification: an inflammatory disease. Circulation journal : official journal of the Japanese Circulation Society. 2011; 75(6):1305–13. [PubMed: 21566338]
9. Vickers KC, Castro-Chavez F, Morrisett JD. Lyso-phosphatidylcholine induces osteogenic gene expression and phenotype in vascular smooth muscle cells. Atherosclerosis. 2010; 211(1):122–9. [PubMed: 20451909]
10. Castro-Chavez F, Vickers KC, Lee JS, Tung CH, Morrisett JD. Effect of lyso-phosphatidylcholine and Schnurri-3 on osteogenic transdifferentiation of vascular smooth muscle cells to calcifying vascular cells in 3D culture. Biochimica et biophysica acta. 2013; 1830(6):3828–34. [PubMed: 23500015]
11. Ababneh B, Rejjal L, Pokharel Y, Nambi V, Wang X, Tung C-H, et al. Distribution of Calcification in Carotid Endarterectomy Tissues: Comparison of micro-Computed Tomography Imaging to Histology. Vascular Medicine. 2014; 19(5):343–50. [PubMed: 25193489]
12. Huang H, Virmani R, Younis H, Burke AP, Kamm RD, Lee RT. The impact of calcification on the biomechanical stability of atherosclerotic plaques. Circulation. 2001; 103(8):1051–6. [PubMed: 11222465]
13. Shaalan WE, Cheng H, Gewertz B, McKinsey JF, Schwartz LB, Katz D, et al. Degree of carotid plaque calcification in relation to symptomatic outcome and plaque inflammation. J Vasc Surg. 2004; 40(2):262–9. [PubMed: 15297819]

14. Kelly-Arnold A, Maldonado N, Laudier D, Aikawa E, Cardoso L, Weinbaum S. Revised microcalcification hypothesis for fibrous cap rupture in human coronary arteries. Proceedings of the National Academy of Sciences of the United States of America. 2013; 110(26):10741–6. [PubMed: 23733926]
15. Vengrenyuk Y, Carlier S, Xanthos S, Cardoso L, Ganatos P, Virmani R, et al. A hypothesis for vulnerable plaque rupture due to stress-induced debonding around cellular microcalcifications in thin fibrous caps. Proceedings of the National Academy of Sciences of the United States of America. 2006; 103(40):14678–83. [PubMed: 17003118]
16. Mauriello A, Servadei F, Sangiorgi G, Anemona L, Giacobbi E, Liotti D, et al. Asymptomatic carotid plaque rupture with unexpected thrombosis over a non-canonical vulnerable lesion. Atherosclerosis. 2011; 218(2):356–62. [PubMed: 21813127]
17. Wiltz DC, Han RI, Wilson RL, Kumar A, Morrisett JD, Grande-Allen KJ. Differential Aortic and Mitral Valve Interstitial Cell Mineralization and the Induction of Mineralization by Lysophosphatidylcholine. Cardiovascular engineering and technology. 2014; 5(4):371–83. [PubMed: 25419248]
18. Ciccone MM, Marzullo A, Mizio D, Angiletta D, Cortese F, Scicchitano P, et al. Can carotid plaque histology selectively predict the risk of an acute coronary syndrome? International heart journal. 2011; 52(2):72–7. [PubMed: 21483163]
19. Higgins CL, Isbilir S, Basto P, Chen IY, Vaduganathan M, Vaduganathan P, et al. Distribution of Alkaline Phosphatase, Osteopontin, RANK Ligand and Osteoprotegerin in Calcified Human Carotid Atheroma. The protein journal. 2015; 34(5):315–28. [PubMed: 26307009]
20. Jeziorska M, McCollum C, Woolley DE. Calcification in atherosclerotic plaque of human carotid arteries: associations with mast cells and macrophages. The Journal of pathology. 1998; 185(1): 10–7. [PubMed: 9713354]
21. Bini A, Mann KG, Kudryk BJ, Schoen FJ. Noncollagenous bone matrix proteins, calcification, and thrombosis in carotid artery atherosclerosis. Arteriosclerosis, thrombosis, and vascular biology. 1999; 19(8):1852–61.
22. Meloan SN, Puchtler H. Chemical Mechanisms of Staining Methods: Von Kossa's Technique: What von Kossa Really Wrote and a Modified Reaction for Selective Demonstration of Inorganic Phosphate. J Histotechol. 1985; (1):11–3.
23. Bertazzo S, Gentleman E, Cloyd KL, Chester AH, Yacoub MH, Stevens MM. Nano-analytical electron microscopy reveals fundamental insights into human cardiovascular tissue calcification. Nature materials. 2013; 12(6):576–83. [PubMed: 23603848]
24. Miller JD. Cardiovascular calcification: Orbicular origins. Nature materials. 2013; 12(6):476–8. [PubMed: 23695741]
25. Vickers KC, Maguire CT, Wolfert R, Burns AR, Reardon M, Geis R, et al. Relationship of lipoprotein-associated phospholipase A2 and oxidized low density lipoprotein in carotid atherosclerosis. J Lipid Res. 2009; 50(9):1735–43. [PubMed: 19359705]
26. Abedin M, Tintut Y, Demer LL. Vascular calcification: mechanisms and clinical ramifications. Arteriosclerosis, thrombosis, and vascular biology. 2004; 24(7):1161–70.
27. Glagov S, Zarins C, Giddens DP, Ku DN. Hemodynamics and atherosclerosis. Insights and perspectives gained from studies of human arteries. Archives of pathology & laboratory medicine. 1988; 112(10):1018–31. [PubMed: 3052352]
28. Giddens DP, Zarins CK, Glagov S. The role of fluid mechanics in the localization and detection of atherosclerosis. Journal of biomechanical engineering. 1993; 115(4B):588–94. [PubMed: 8302046]
29. Wahlgren CM, Zheng W, Shaalan W, Tang J, Bassiouny HS. Human carotid plaque calcification and vulnerability. Relationship between degree of plaque calcification, fibrous cap inflammatory gene expression and symptomatology. Cerebrovascular diseases. 2009; 27(2):193–200. [PubMed: 19136823]
30. Zarins CK, Giddens DP, Bharadvaj BK, Sottiurai VS, Mabon RF, Glagov S. Carotid bifurcation atherosclerosis. Quantitative correlation of plaque localization with flow velocity profiles and wall shear stress. Circ Res. 1983; 53(4):502–14. [PubMed: 6627609]

31. Pasterkamp G, de Kleijn DP, Borst C. Arterial remodeling in atherosclerosis, restenosis and after alteration of blood flow: potential mechanisms and clinical implications. Cardiovascular research. 2000; 45(4):843–52. [PubMed: 10728409]
32. Korshunov VA, Berk BC. Strain-dependent vascular remodeling: the “Glagov phenomenon” is genetically determined. Circulation. 2004; 110(2):220–6. [PubMed: 15226209]
33. Saam T, Ferguson MS, Yarnykh VL, Takaya N, Xu D, Polissar NL, et al. Quantitative evaluation of carotid plaque composition by in vivo MRI. Arteriosclerosis, thrombosis, and vascular biology. 2005; 25(1):234–9.
34. Lehto S, Niskanen L, Suhonen M, Ronnemaa T, Laakso M. Medial artery calcification. A neglected harbinger of cardiovascular complications in non-insulin-dependent diabetes mellitus. Arteriosclerosis, thrombosis, and vascular biology. 1996; 16(8):978–83.
35. Shanahan CM, Cary NR, Salisbury JR, Proudfoot D, Weissberg PL, Edmonds ME. Medial localization of mineralization-regulating proteins in association with Monckeberg’s sclerosis: evidence for smooth muscle cell-mediated vascular calcification. Circulation. 1999; 100(21): 2168–76. [PubMed: 10571976]
36. McCullough PA, Chinnaiyan KM, Agrawal V, Danielewicz E, Abela GS. Amplification of atherosclerotic calcification and Monckeberg’s sclerosis: a spectrum of the same disease process. Advances in chronic kidney disease. 2008; 15(4):396–412. [PubMed: 18805386]
37. Anderson HC. Mineralization by matrix vesicles. Scan Electron Microsc. 1984; (Pt 2):953–64. [PubMed: 6385226]
38. Shao JS, Cai J, Towler DA. Molecular mechanisms of vascular calcification: lessons learned from the aorta. Arteriosclerosis, thrombosis, and vascular biology. 2006; 26(7):1423–30.
39. Wang Y, Johnson JA, Fulp A, Sutton MA, Lessner SM. Adhesive strength of atherosclerotic plaque in a mouse model depends on local collagen content and elastin fragmentation. Journal of biomechanics. 2013; 46(4):716–22. [PubMed: 23261250]
40. Newby AC. Dual Role of Matrix Metalloproteinases (Matrixins) in Intimal Thickening and Atherosclerotic Plaque Rupture. Physiol Rev. 2005; 85(1):1–31. [PubMed: 15618476]
41. Virmani R, Burke AP, Kolodgie FD, Farb A. Pathology of the thin-cap fibroatheroma: a type of vulnerable plaque. JIntervCardiol. 2003; 16(3):267–72.
42. Niccoli Asabella A, Ciccone MM, Cortese F, Scicchitano P, Gesualdo M, Zito A, et al. Higher reliability of 18F-FDG target background ratio compared to standardized uptake value in vulnerable carotid plaque detection: a pilot study. Annals of nuclear medicine. 2014; 28(6):571–9. [PubMed: 24737136]

Highlights

- Calcification is abundant in carotid endarterectomy (CEA) tissues
- Calcification is located predominantly in the bulb/bifurcation segment of CEAs
- Histologically determined calcified patch sizes span across 4-orders of magnitude
- Morphology of calcified patches changes significantly with patch size

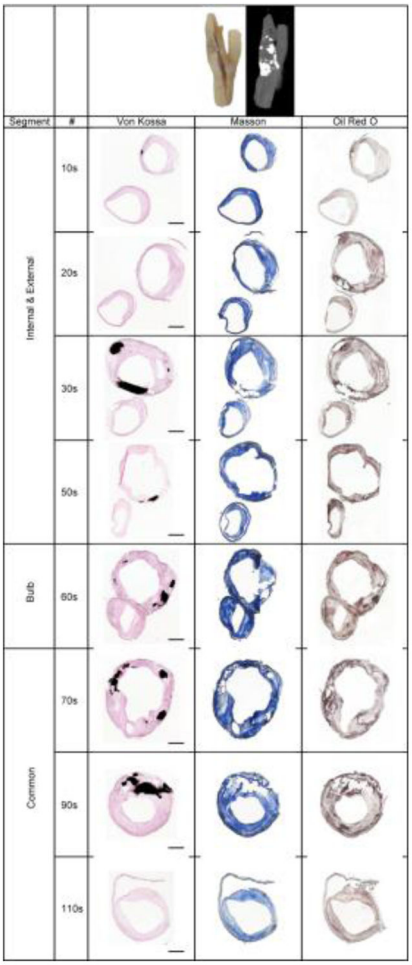

Figure 1.

A representative example of a macro tissue and its corresponding μ-CT images plus warped and morphed histological image showing the common, internal, external and bulb segments along the axis of a right CEA. Rupture of the calcified patches due to sectioning is evident, leaving the remnant of calcified fragments near the edge. The space void of calcified patch was rendered in black to show the entire calcified area in von Kossa images. # = tissue section number from distal side. Von Kossa: black = calcium phosphate; Masson's trichrome: blue = collagen, red = fibrin; Oil Red O, red = lipid. Scale bar = 2mm.

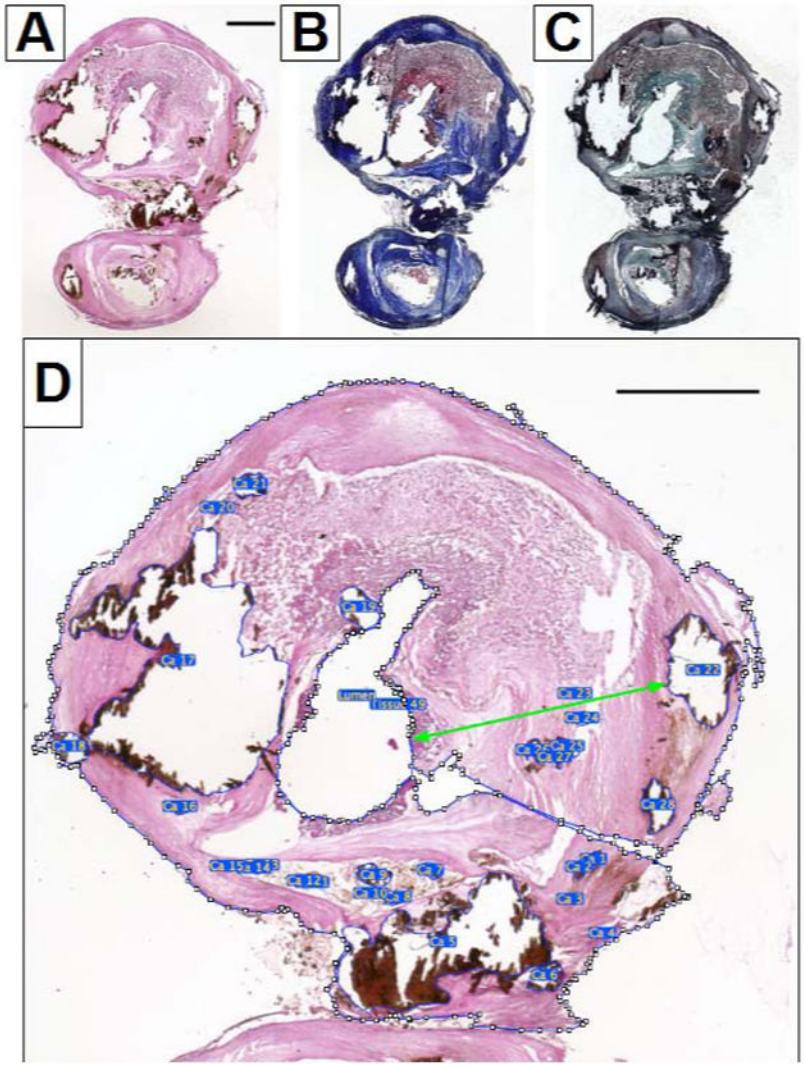

Figure 2.

Whole slide-scanned micrographs of a left CEA tissue near the bifurcation to illustrate the composition of an atherosclerotic plaque. Scale bar = 2mm. A): von Kossa staining shows the calcium phosphate in black. B): Masson's trichrome staining shows the collagen in blue and fibrin in red. C): Oil Red O with Verhoeff counter staining shows the lipid in red and elastin in blue/black. D): A close up view of the internal segment of the von Kossa stained CEA tissue, the polygon selection function of the ImageJ software was used to delineate the lumen, tissue area and every calcified patch. The green double arrow line indicating the fibrous layer thickness for calcium patch number 22 (Ca 22). The lumen shape was irregular and lumen area was constricted.

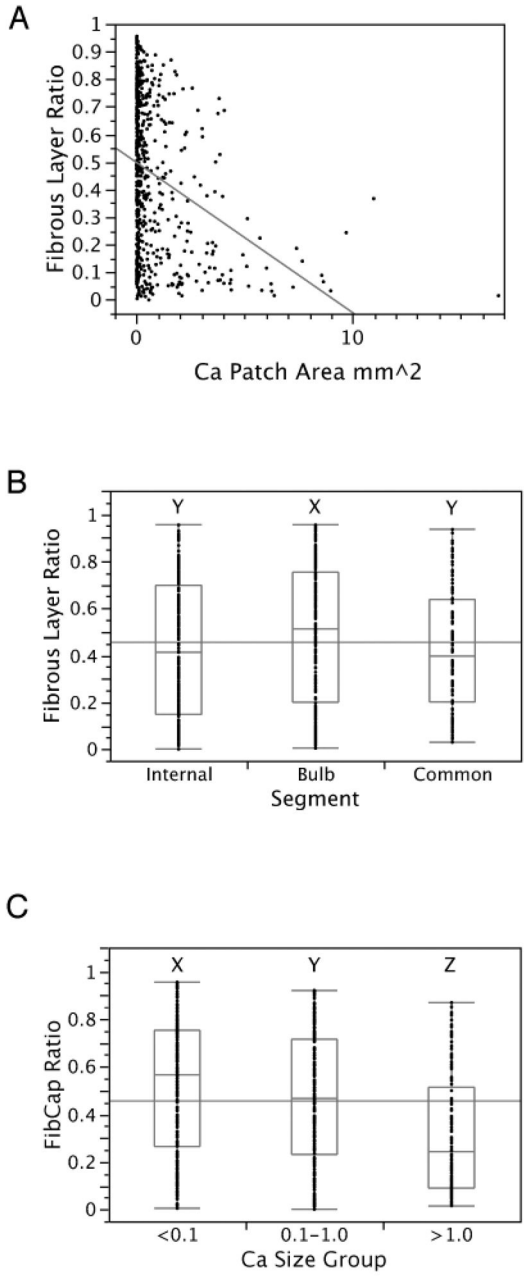

Figure 3.

A:) Bivariant graph between calcium patch area (n=622) and fibrous layer thickness ratio, linear extrapolation showed an inverse relationship. B:) Fibrous layer thickness ratios in internal (n=244), bulb (n=276), and common (n=102) segments. C:) Fibrous layer thickness ratios in <0.1mm^2 (n=279), 0.1–1.0mm^2 (n=210), and >1.0mm^2 (n=133) size groups. The difference between groups is shown by the letter (X, Y or Z) above each group, where a shared letter indicates no significant difference (Tukey-Kramer pairwise analysis).

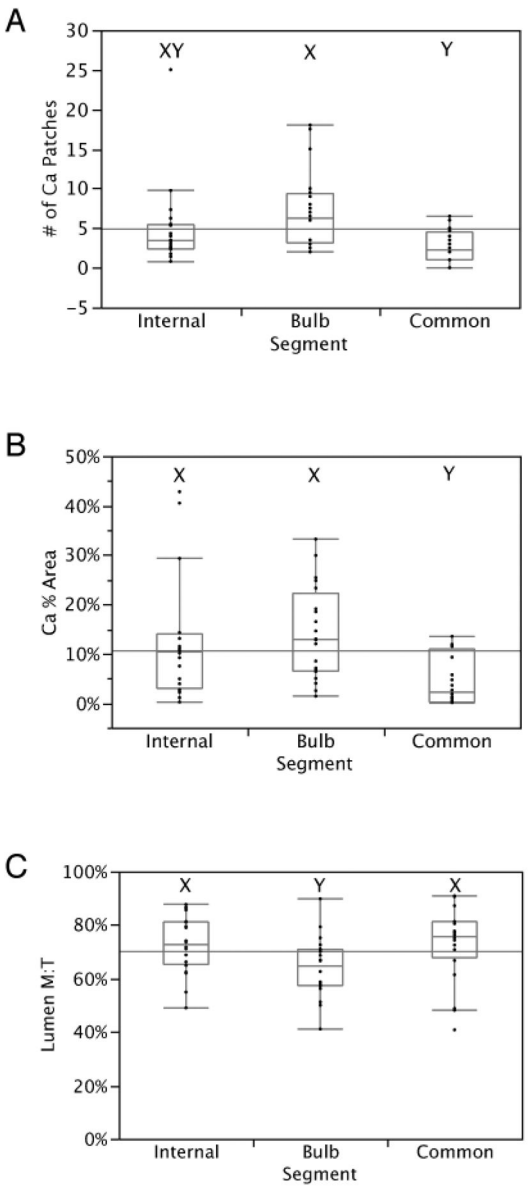

Figure 4.

Box and whiskers plots illustrating the mean, upper and lower quartile of the (A) number of calcified patches; (B) calcified area as a % of total tissue; (C) ratio of measured lumen area to hypothetical lumen area (M: measured, T: theoretical), between internal, bulb, and common segments of combined CEA (Lt+Rt). The difference between segment groups is shown by the letter (X, Y or XY) above each group, where a shared letter indicates no significant difference (Tukey-Kramer pairwise analysis).

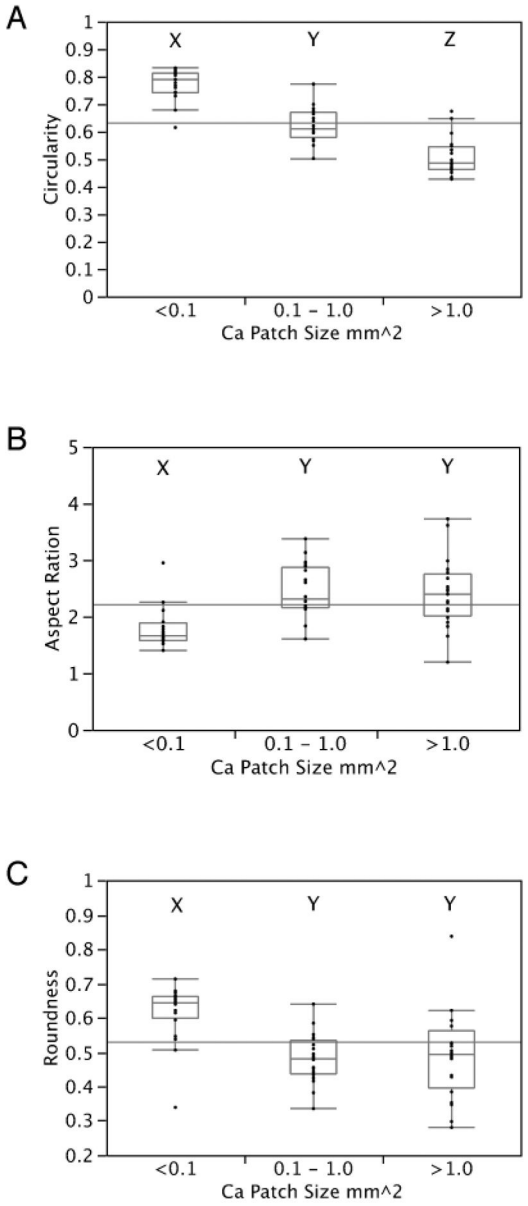

Figure 5.

Box and whiskers plots illustrating the mean, upper and lower quartile of the shape descriptors for combined CEA (Lt+Rt) calcified patches in three different size groups (<0.1, 0.1–1.0 and >1.0 mm^2). (A) The circularity, a measure of calcified patch shape outline. (B) Aspect ratio, a measure of growth in x- and y- directions. (C) Roundness, a measure of eccentricity. The difference between calcium patch size groups is shown by the letter above each group (X, Y or Z), where a shared letter indicates no significant difference (Tukey-Kramer pairwise analysis).

Figure 6.

A representative von Kossa stained CEA tissue section of the bulb segment as show at different magnifications to illustrate the very-small calcified particles (bar, A: 5000μm, B: 500μm and C: 50μm). The very small calcified particles are rounded in shape, but some are coalescing with each other to form a bigger particle (green arrow insert).

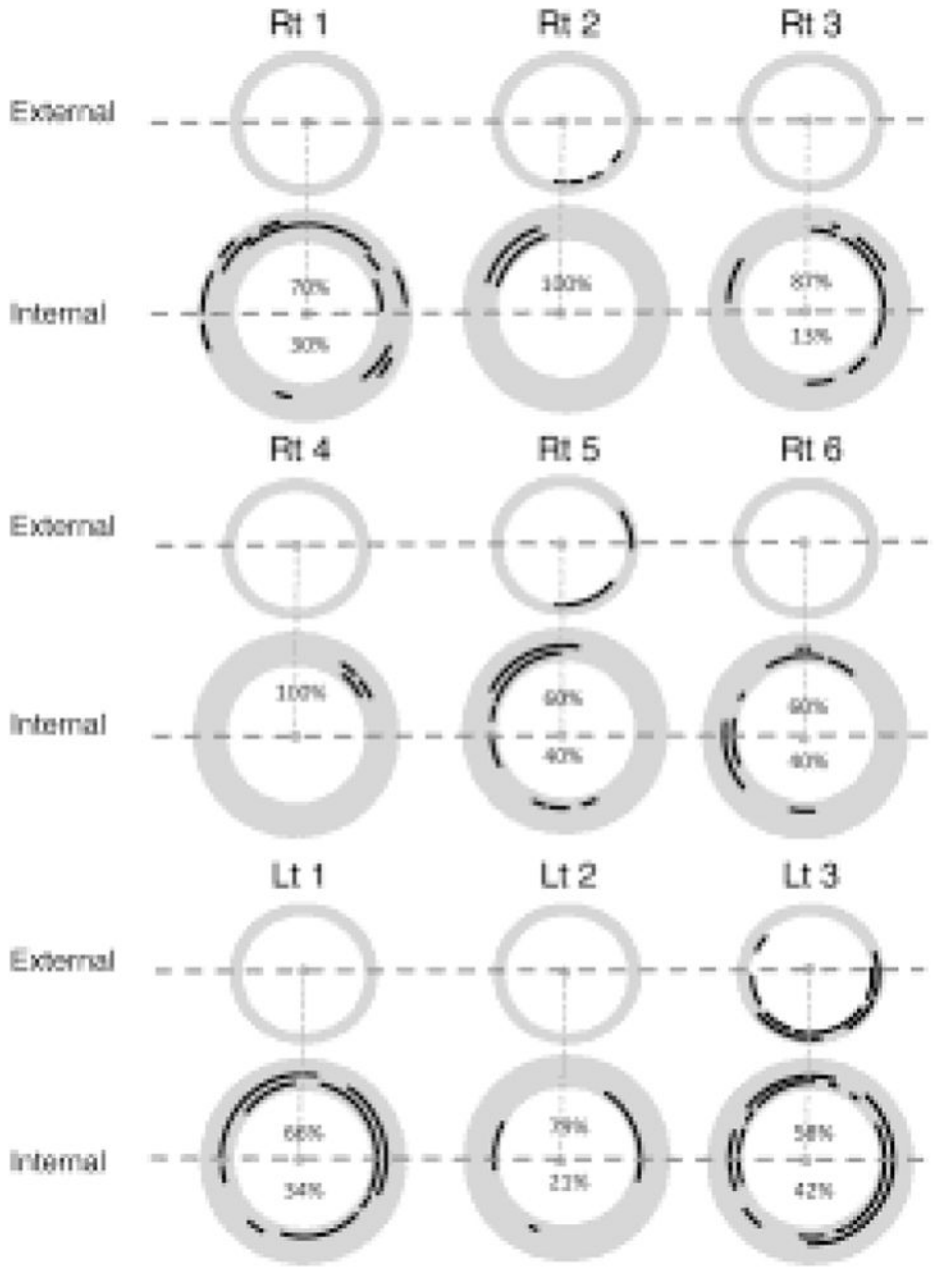

Figure 7.

Radial distribution of calcified patches in the external and internal branches of 9 CEA tissues. A black arc around the concentric circle represents the angle occupation by the calcified particle. The arcs in the same concentric circle represented the calcified particles located on the same tissue section. The outer rim represented the proximal side, and the inner rim represented distal side. The dotted line is perpendicular to the reference line (joins the centroids of the two lumens) and intersects the centroid of the internal lumen. The calcification area in each halves is expressed as a percentage of total calcification area. Rt: Right; Lt: Left.